Available online at www.sciencedirect.com
ScienceDirect
Nuclear Physics B (Proc. Suppl.) 190 (2009) 5–11
NUCLEAR PHYSICS B PROCEEDINGS SUPPLEMENTS
www.elsevierphysics.com

Overview of Recent HiRes Results

J. Belz[a*], *for the HiRes Collaboration*

[a]Department of Physics, University of Utah, Salt Lake City, Utah 84112, U.S.A.

We present an overview of the most recent results from the High-Resolution Fly's Eye (HiRes) observatory. These include both monocular and stereo energy spectra, the results of a search for correlations between event arrival directions and active galactic nuclei, and new results on composition studies using airshower maximum.

1. THE HIGH RESOLUTION FLY'S EYE

The High Resolution Fly's Eye (HiRes) observatory was operated from May 1997 to April 2006 on the Dugway Proving Grounds in Utah, U.S.A. HiRes consisted of two nitrogen fluorescence detectors: HiRes-I at (40.2° N, 112.8° W, 1597 meters M.S.L.) and HiRes-II at (40.1° N, 113.0° W, 1553 meters M.S.L.), separated by approximately 13 km.

HiRes-I consisted of a single ring of fluorescence cameras viewing elevation angles from 3° to 17°. HiRes-II, which became operational in December 1999, consisted of two rings of cameras viewing elevation angles from 3° to 31°. Each camera consisted of a 16×16 array of photomultiplier tubes (PMTs) at the focus of a 4 m^2 spherical mirror. HiRes-II also made use of a 100 ns clock flash ADC aystem [1], which allowed grouping of PMT pulse-height information from different tubes with the same hit times. This feature played an important role in the analyses described in this paper.

2. ENERGY SPECTRA

Reconstruction of airshower events proceeds by using the fluorescence light signal to infer the number of charged particles as a function of depth in the atmosphere (Figure 1). By comparing the profiles of observed events to CORSIKA [2] simulated airshower events, primary particle energy and airshower characteristics (including X_{max}) are estimated.

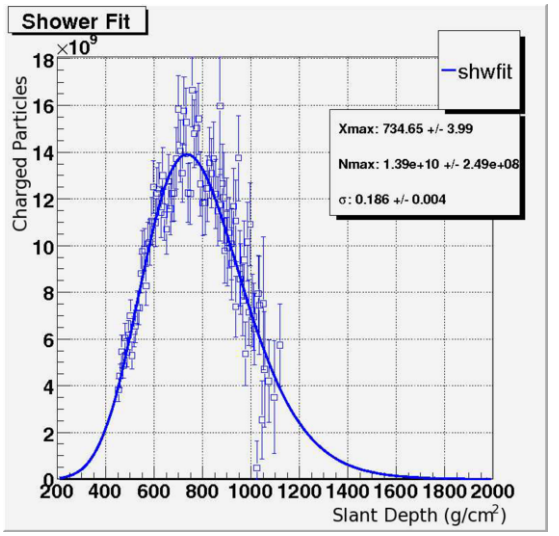

Figure 1. Shower profile of HiRes stereoscopic event. Phototube pulses are sorted into time bins, the y-axis is converted from fluorescence light output (proportional to energy deposition) to the number of charged particles assuming an average energy deposition per particle of 2.4 MeV/g cm^2.

HiRes recently reported the first observation at the 5σ level of the GZK [3] suppression feature in monocular measurements of the ultra-high energy cosmic ray spectrum [4]. This result, confirming a 40 year old prediction, establishes the extragalactic nature of the highest energy cosmic rays.

HiRes however was designed as a stereo fluorescence experiment, and obtains its best event reconstruction in stereoscopic mode. The stereo

*electronic address: belz@cosmic.utah.edu

0920-5632/$ – see front matter
doi:10.1016/j.nuclphysbps.2009.03.061

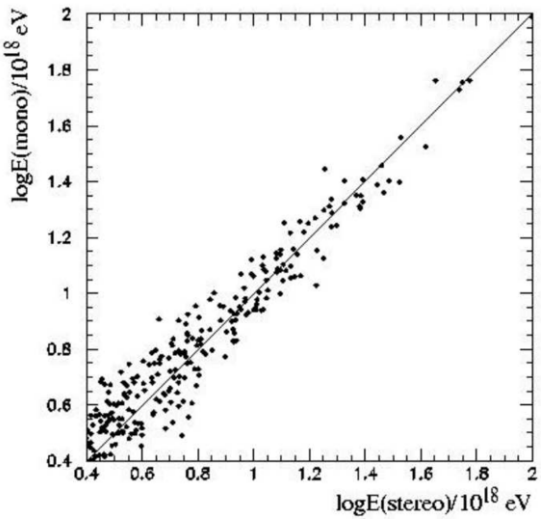

Figure 2. HiRes-I monocular energy versus stereo energy, for the subset of events reconstructed in both modes.

event sample, while consisting of fewer events, can thus serve as an important confirmation of the monocular results as well as a check of monocular systematic uncertainties. Figure 2 illustrates the consistency of HiRes-I monocular and stereo energy measurements for individual events.

Major systematic uncertainties in the stereo energy measurements are given in Table 1. The photometric calibration of the HiRes telescopes has been described previously [5], and is based on a xenon flash lamp that is placed at the center of each mirror which illuminates the phototube camera. The intensity of fluorescence light emitted

Table 1
Systematic uncertainties in HiRes stereo energy spectrum

Item	Uncertainty
Photonic scale	10%
Fluorescence yield	6%
Deposited energy calculation	10%
Aerosol concentration	6%
TOTAL	17%

from a cosmic ray shower is proportional to the total ionization energy deposited by the charged particles in the shower [6]. We have used an average of the fluorescence yield measurements from the first three papers of reference [7]; Our fluorescence uncertainty is derived from the averaging procedure.

We estimate a systematic uncertainty of 10% from the energy deposition model used in determining the charged particle counts from the fluorescence signal. Our last major systematic uncertainty comes from variability of the aerosol concentrations, an effect minimized by monitoring of aerosols at the HiRes site on an hourly basis.

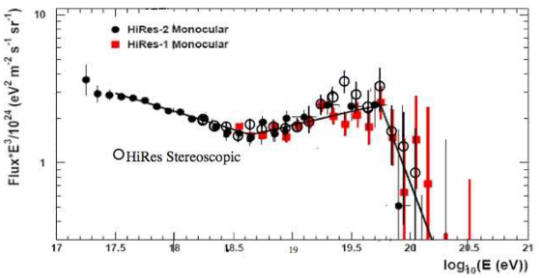

Figure 3. HiRes monocular (black circles and red squares) and stereoscopic (open circles) spectra.

The HiRes monocular and stereo spectra are illustrated in Figure 3. The stereo spectrum is consistent in both magnitude and shape to the monocular spectra, confirming the finding of both an "ankle" at $\log E(eV) = 18.6$ and a high-energy cutoff at $\log E(eV) = 19.7$.

3. Anisotropy: AGN CORRELATIONS

Motivated by the finding of the Pierre Auger Observatory (PAO) [8] of correlations between UHECR arrival directions and Southern Hemisphere Active Galactic Nuclei (AGN) from the 12th Véron catalog [9] , we report the results for of a similar search in the Northern Hemisphere.

The PAO AGN signal was established in an exploratory scan of data collected between January 2004 and May 2006. In this scan, it was established that requiring that the opening angle $\theta < 3.1°$, the energy $E > 56$ EeV, and AGN redshift $Z < 0.018$ maximized the correlation of UHECR arrival directions with AGN. A subsequent sequential analysis of independent events collected between June 2006 and August 2007 found correlations between AGN and 8 of 13

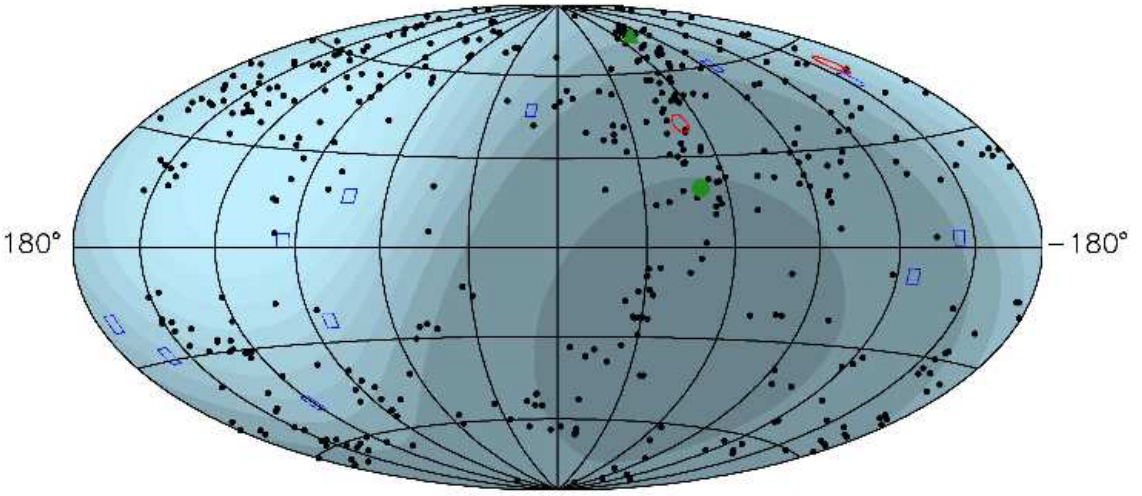

Figure 4. Sky map in galactic coordinates. Black circles: AGN with $Z < 0.018$. Blue squares: uncorrelated HiRes stereo events above 56 EeV. Red circles: HiRes stereo events within a space angle $\theta < 3.1°$ of a candidate AGN. The green circle represents Cen A, and the green triangle represents M87. The blue shaded regions delineate regions of constant exposure, the darkest indicating no exposure.

events above 56 EeV. Accounting for the statistical effects of the sequential analysis, the chance probability of such an effect was estimated to be approximately 1%.

The HiRes AGN analysis consisted of two parts, a direct test of the PAO criteria as well as an independent scan of the HiRes stereo dataset. For the direct test, HiRes event energies were shifted downwards by 10% to correct for an apparent energy scale mismatch between the two experiments [4, 10]. The results of this search are shown in Figure 4. Using the scan criteria established by the PAO, HiRes finds 2 of 13 events above 56 EeV correlate with AGNs, where 3.2 are expected randomly. With a chance probability of 83%, the HiRes data is consistent with no correlation effect.

In a second test of the AGN-as-source hypothesis, we conducted an independent scan of the HiRes stereo data using the method suggested by Finley and Westerhoff [11]. We find the most significant effect occurs at the opening angle $\theta < 2.0°$, the energy $E > 16$ EeV, and AGN redshift $Z < 0.016$. Using this criteria, 36/198 events have their arrival directions correlate with AGN. The chance probability of this correlation is 24%, hence we conclude that the HiRes data is consistent with no significant deviation from isotropy.

Taken together, these findings weaken the general AGN hypothesis, while making no statement about Southern Hemisphere AGN. This result was recently published by HiRes [12].

4. COMPOSITION WITH X_{max}

A simple extension [13] of Heitler's model for electromagnetic cascades [14] shows that we can expect the average value of *airshower maximum* $<X_{max}>$ to follow the relation

$$<X_{max}> = \lambda_r \left(\ln \frac{E}{\xi_c^e} - \ln A \right) + C \qquad (1)$$

where λ_r is the radiation length of the medium (air), ξ_c^e the critical energy (at which radiative energy loss equals collisional energy loss), and E and and A are respectively the energy and atomic mass of the primary cosmic ray. C is model-dependent, and approximately independent of energy.

Differentiating this relation we obtain the *elongation rate* Λ_A

$$\Lambda_A = \frac{d <X_{max}>}{d \log E} \approx \lambda_r \left(2.3 - \frac{d \ln A}{d \log E} \right) \qquad (2)$$

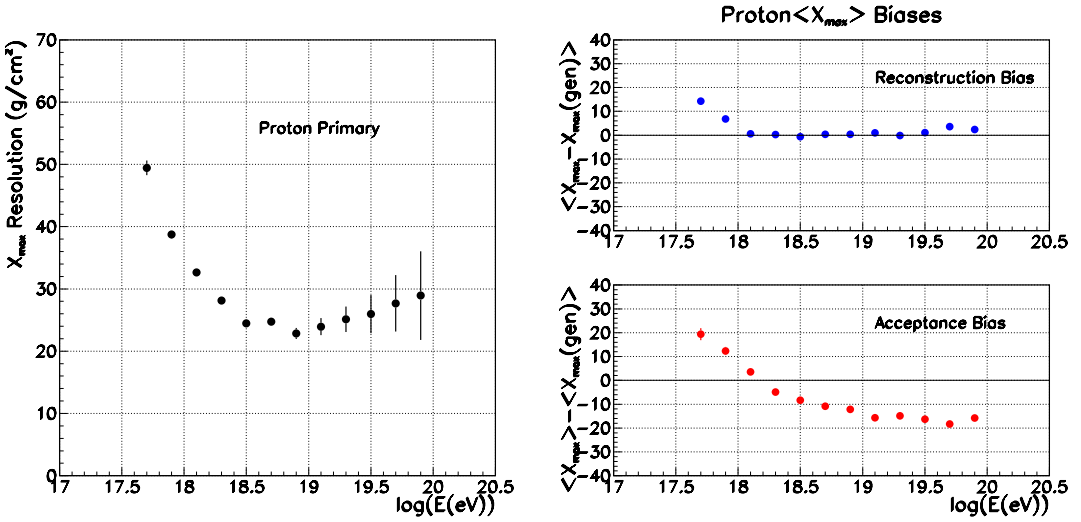

Figure 5. *Left:* X_{max} resolution for airshowers initiated by proton primary cosmic rays, as determined using a QGSJET01 shower library and the HiRes detector Monte Carlo. *Right:* $<X_{max}>$ reconstruction (top) and acceptance (bottom) biases for QGSJET01 proton Monte Carlo, after application of all cuts applied in the text.

which is a common choice as a composition discriminant because of its simple dependence on A.

We derive X_{max} from a shower (Figure 1) by recasting the charged particle profile in terms of the age parameter:

$$s = \frac{3X}{X + 2X_{max}} \tag{3}$$

and fitting the result to a Gaussian distribution with X_{max} as its peak. We find the Gaussian-In-Age (GIA) functional form to have smaller residuals over the fit range than the more commonly used Gaisser-Hillas (GH) parametrization [15], and that the GIA parametrization results in more stable fits.

For comparison with airshower model predictions, we make use of a QGSJET01 shower library, consisting of both proton and iron-initiated airshowers. Before being propagated through the HiRes detector Monte Carlo, we determine the model predictions for $<X_{max}>$ by fitting the *thrown* proton and iron shower profiles to the same GIA function used in event reconstruction. The results of these fits are given in Table 2.

The critical issue in comparing experimental $<X_{max}>$ distributions to the model predictions lies in understanding the various biases that the detector acceptance and reconstruction programs can impart on the data. It is useful to categorize these biases into two types:

Table 2
QGSJET-I predictions for $<X_{max}>$.

Primary	Elongation Rate	$<X_{max}>$ at $\log E = 19.0$
proton	47.9 g/cm^2/decade	763.2 g/cm^2
iron	58.9 g/cm^2/decade	683.0 g/cm^2

1. *Reconstruction bias*: Due to events which are successfully reconstructed and pass data quality cuts which have the wrong X_{max}.

2. *Acceptance bias*: Due to events which fail reconstruction altogether, at preferentially shallow or deep levels in the atmosphere.

The current analysis takes the approach of choosing the simplest cuts consistent with obtaining minimal reconstruction bias, and then applying acceptance corrections to the data in order to arrive at an elongation rate which can be compared to predictions.

Event geometry for this study is determined using both the HiRes-I and HiRes-II detector sites. Only the HiRes-II information is used in forming the shower profile. All events are required to undergo a successful profile fit, in addition to:

- having a zenith angle $< 70°$
- having X_{max} be "bracketed" by the observed bins
- having the shower impact parameter with respect to HiRes-II be greater than 5 km
- having the angle of the airshower in the HiRes-II shower-detector plane ψ satisfy the condition $40° < \psi < 130°$

The X_{max} resolution for HiRes stereo events satisfying the above criteria is illustrated in Figure 5 (left).

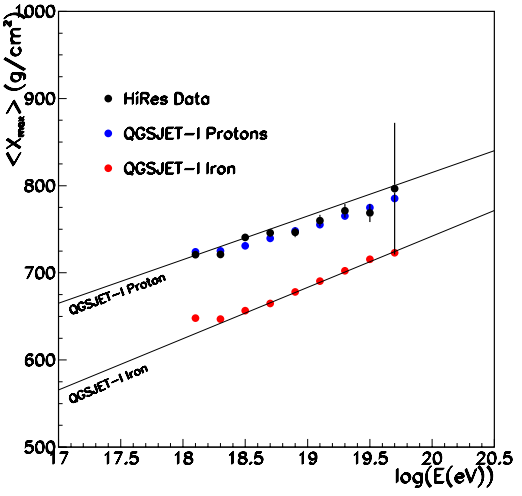

Figure 6. $<X_{max}>$ for the HiRes stereo data, along with QGSJET01 proton and iron showers passing through a detector Monte Carlo and the full analysis chain. Also shown are the "rails" (Table 2) from the shower library predictions. Acceptance corrections have not yet been applied.

Figure 5 (right) illustrates the reconstruction and acceptance biases, as determined from

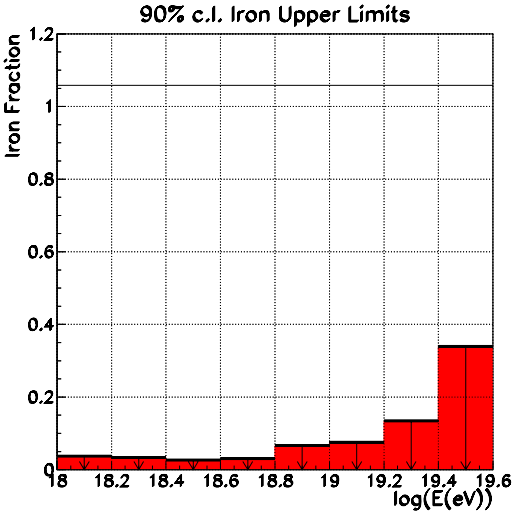

Figure 7. 90% c.l. upper limits on the iron fraction in the data, within the QGSJET01 two-component ansatz. A likelihood fit is performed in which the X_{max} distribution in the data (in each energy range) is compared to a sum of QGSJET01 proton and iron distributions.

QGSJET01 proton Monte Carlo, after application of the above criteria. There is essentially no reconstruction bias above 1 EeV. Below this, we see the effects of shallow showers being reconstructed systematically deeper than they actually are, as at their true depth they would fail the bracketing requirement. As Figure 5 (right) also shows, there remains an acceptance bias of approximately 15 g/cm^2 at the highest energies, for which we will later correct.

$< X_{max} >$ for the HiRes stereo data, along with QGSJET01 proton and iron showers passing through a detector Monte Carlo and the full analysis chain, are shown in Figure 6. The data is clearly most like the QGSJET01 proton prediction. Figure 7 shows the result of fitting the X_{max} distributions in a given energy bin to a sum of QGSJET01 proton and iron distributions. Under this ansatz, we place 90% c.l. upper limits on the iron fraction of less than 0.1 over most of the HiRes energy range.

Finally, to do a direct comparison with the shower library predictions as well as to determine experimental values for $<X_{max}>$ and the elonga-

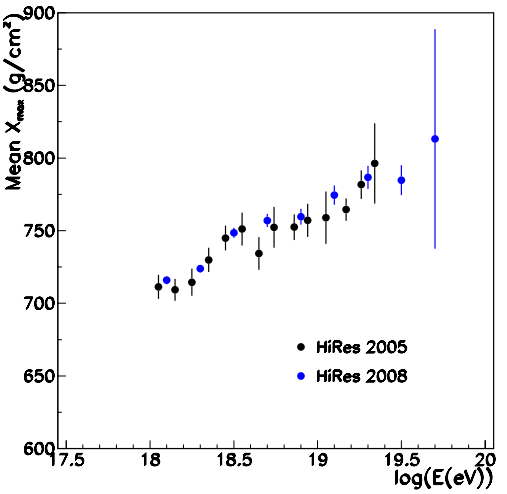

Figure 8. Current HiRes $<X_{max}>$ result (blue points), after acceptance correction is applied, superimposed on previously published HiRes results (black points) [16].

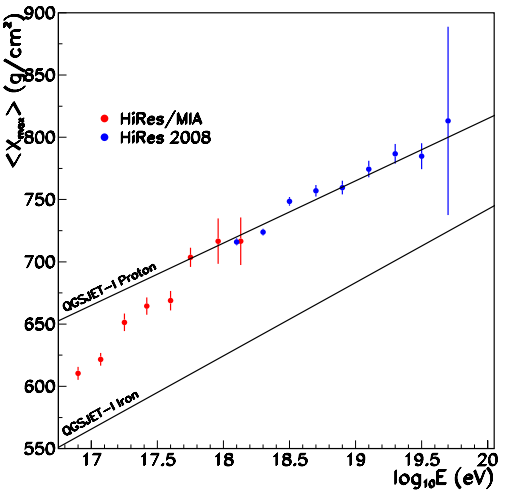

Figure 9. Current HiRes $<X_{max}>$ result (blue points), after acceptance correction is applied, superimposed on previously published HiRes prototype/MIA results (red points) [17]. Also shown are QGSJET01 predictions for protons and iron.

tion rate we perform an acceptance correction to the data using the QGSJET01 proton prediction. Results are shown in Figure 8. Results agree well with previous HiRes published data, within uncertainties. Figure 9 overlays the present result with that of the hybrid HiRes prototype/MIA array [17]. The apparent change in elongation rate in the 0.1–1.0 EeV decade is a strong motivation for future experiments such as the TALE [18] project, which seek to understand the composition of primary UHECR over the full range of energies contained in this plot.

5. Acknowledgements

This work is supported by US NSF grants PHY-9321949, PHY-9322298, PHY-9904048, PHY-9974537, PHY-0098826, PHY-0140688, PHY-0245428, PHY-0305516, PHY-0307098, and by the DOE grant FG0392ER40732. We gratefully acknowledge the contributions from the technical staffs of our home institutions. The cooperation of Colonels E. Fisher, G. Harter and G. Olsen, the US Army, and the Dugway Proving Ground staff is greatly appreciated.

REFERENCES

1. J. H. Boyer *et al.*, *Nucl. Instrum. Methods* **A482** 457 (2002).
2. D. Heck *et al.*, CORSIKA: A Monte Carlo code to simulate extensive air showers, Forschungszentrum Karlsruhe technical note FZKA 6019 (1998).
3. K. Greisen, *Phys. Rev. Lett.* **16** 748 (1966).
   G. Zatsepin and V. Kuz'min, *J. Exp. Theor. Phys. Lett* **4** 78 (1966).
   G. Zatsepin and V. Kuz'min, *J. Exp. Theor. Phys. Lett* **4** 114 (1966).
4. R. Abbasi *et al.*, *Phys. Rev. Lett.* **100** 101101 (2008).
5. R. Abbasi *et al.*, *Astropart. Phys.* **23**, 157 (2005).
6. J.W. Belz *et al.*, *Astropart. Phys.* **25**, 57 (2006).
7. F. Kakimoto *et al.*, *Nucl. Instrum. Meth.* **A** (1996)
   M. Nagano *et al.*, *Astropart. Phys.* **20**, 293 (2003).
   J.W. Belz *et al.*, *Astropart. Phys.* **25**, 129 (2006).

A.N. Bunner, Ph.D. thesis, Cornell University, 1967.
8. J. Abraham *et al.*, *Science*, **318** 938 (2007). J. Abraham *et al.*, *Astropart. Phys.*, **29** 188 (2008).
9. M.P. Véron-Cetty and P. Véron, *Astron. Astrophys.* **455** 773 (2006).
10. J. Abraham *et al.*, *Phys. Rev. Lett.*, **101** 061101 (2008).
11. C. Finley and S. Westerhoff, *Astropart. Phys.* **21**, 359 (2004).
12. R. Abbasi *et al.*, *Astropart. Phys.* **30** 175 (2008).
13. J. Matthews, *Astropart. Phys.* **22** 387 (2005).
14. W. Heitler, *The Quantum Theory of Radiation*, Oxford University Press (1954).
15. T. Gaisser and A. Hillas, *Proc. 15th ICRC, Plovdiv, Bulgaria* **12** 89 (1977).
16. R. Abbasi *et al.*, *Ap. J.* **622** 910 (2005).
17. T. Abu-Zayyad *et al.*, *Phys. Rev. Lett.* **84** 4276 (2000).
18. J. Matthews, proceedings of this conference.